HOKKAIDO UNIVERSITY

Title	Influence of bias voltage on the performance of polarization-sensitive near-infrared photodiode based on dilute nitride GaNAs
Author(s)	Mineyama, Daiki; Yano, Tatsuya; Etou, Kohei et al.
Citation	Applied physics letters, 126(22), 223507 https://doi.org/10.1063/5.0269453
Issue Date	2025-06-02
Doc URL	https://hdl.handle.net/2115/97910
Rights	This article may be downloaded for personal use only. Any other use requires prior permission of the author and AIP Publishing. This article appeared in Daiki Mineyama, Tatsuya Yano, Kohei Etou, Kaito Nakama, Hidetoshi Hashimoto, Keisuke Minehisa, Junichi Takayama, Agus Subagyo, Kazuhisa Sueoka, Fumitaro Ishikawa, Akihiro Murayama, Satoshi Hiura; Influence of bias voltage on the performance of polarization-sensitive near-infrared photodiode based on dilute nitride GaNAs. Appl. Phys. Lett. 2 June 2025; 126 (22): 223507 and may be found at https://doi.org/10.1063/5.0269453.
Type	journal article
File Information	223507_1_5.0269453.pdf

Hokkaido University Collection of Scholarly and Academic Papers : HUSCAP

Applied Physics Letters

RESEARCH ARTICLE | JUNE 04 2025

Influence of bias voltage on the performance of polarization-sensitive near-infrared photodiode based on dilute nitride GaNAs

Daiki Mineyama; Tatsuya Yano; Kohei Etou; Kaito Nakama ; Hidetoshi Hashimoto; Keisuke Minehisa ; Junichi Takayama ; Agus Subagyo; Kazuhisa Sueoka ; Fumitaro Ishikawa ; Akihiro Murayama ; Satoshi Hiura

Check for updates

Appl. Phys. Lett. 126, 223507 (2025)
https://doi.org/10.1063/5.0269453

View Online
Export Citation

09 July 2025 02:04:27



AIP Publishing

Applied Physics Letters ARTICLE pubs.aip.org/aip/apl

Influence of bias voltage on the performance of polarization-sensitive near-infrared photodiode based on dilute nitride GaNAs

Cite as: Appl. Phys. Lett. **126**, 223507 (2025); doi: 10.1063/5.0269453
Submitted: 6 March 2025 · Accepted: 22 May 2025 ·
Published Online: 4 June 2025

View Online Export Citation CrossMark

Daiki Mineyama,[1] Tatsuya Yano,[1] Kohei Etou,[1] Kaito Nakama,[2] Hidetoshi Hashimoto,[2] Keisuke Minehisa,[2] Junichi Takayama,[1] Agus Subagyo,[1] Kazuhisa Sueoka,[1] Fumitaro Ishikawa,[2] Akihiro Murayama,[1] and Satoshi Hiura[1,a)]

AFFILIATIONS

[1]Faculty of Information Science and Technology, Hokkaido University, Sapporo 060-0814, Japan
[2]Research Center for Integrated Quantum Electronics, Hokkaido University, Sapporo 060-0813, Japan

[a)]Author to whom correspondence should be addressed: hiura@ist.hokudai.ac.jp

ABSTRACT

Recent advances in ultrafast light polarization modulation and electrical control of polarization have increased the demand for polarization-sensitive photodetectors to enable polarization-based optical communication systems. The conduction electron population of dilute nitride GaNAs changes with excitation light polarization owing to the spin-dependent recombination of conduction electrons via the dynamic polarization of defect electron spins. However, polarization-sensitive photodetectors that utilize this property are limited to photoconductive devices with a long response time. In this study, we developed a polarization-sensitive near-infrared photodiode based on GaNAs. The influence of light power and bias voltage on the discrimination efficiency between circularly and linearly polarized light was investigated using coupled rate equation analysis for polarization-dependent photocurrent characteristics. At −2.0 V, where the discrimination efficiency reached 1%, the extraction time of the conduction electrons to the electrode was estimated to be 34 ps. This result suggests that the developed polarization-sensitive photodiode can operate at 10 GHz. The discrimination efficiency increased with light power because of the activated spin-selective capture of conduction electrons by spin-polarized defect states for circularly polarized light, whereas it decreased with increasing reverse bias voltage. This low performance originates from suppressed spin-selective capture, which is due to the combination of electric-field-induced spin relaxation and a decrease in the capture efficiency of conduction electrons. This study provides valuable insights into the influence of the bias voltage on the polarization-dependent photocurrent, which is a key challenge to the realization of practical polarization-sensitive photodiodes based on the spin-dependent recombination effect of conduction electrons.

Published under an exclusive license by AIP Publishing. https://doi.org/10.1063/5.0269453

09 July 2025 02:04:27

There has been growing interest in the development of optical devices that modulate light polarization.[1,2] Polarization modulation has advantages over conventional intensity modulation in terms of high-frequency modulation and low-power consumption.[3] Ultrafast polarization modulation at frequencies exceeding 200 GHz has been demonstrated at room temperature.[2] This was accomplished by adding spin-polarized carriers to vertical-cavity surface-emitting lasers, where oscillations of the coupled spin-photon system can be induced. Recently, by integrating ferromagnetic magnetization reversal driven by spin–orbit torque into a spin-polarized light-emitting diode, the spin polarity of electrons injected from the ferromagnetic electrode into the semiconductor was electrically controlled, resulting in circular polarization modulation.[1] Moreover, previous studies have demonstrated that the circular polarization degree of luminescence can be flexibly tuned by controlling the magnetization states. These recent advances in light polarization modulation will enable multilevel modulation for polarization-based optical communications. Photodetectors with the ability to identify light polarization are essential for realizing polarization-based optical communication systems.[4,5]

Recently, discrimination between circularly and linearly polarized light has been achieved at room temperature without a magnetic field using a photoconductor based on dilute nitride GaNAs.[6] This detection method leverages the spin-dependent recombination (SDR) of conduction electrons,[7,8] caused by spin-polarized defect states derived from paramagnetic Ga^{2+} interstitials.[9] First, unpaired non-polarized electron spins exist in the defect states of GaNAs. Subsequently, the

Published under an exclusive license by AIP Publishing

spin-polarized conduction electrons generated by circularly polarized excitation are captured by the defect states. Here, the recombination probability of the defect electron spins with holes is independent of the spin direction; thus, the defect electron spins are dynamically polarized in the same direction as the conduction electron spins. According to the Pauli exclusion rule, defect states cannot capture conduction electrons with the same spin direction, whereas they can capture conduction electrons with the opposite direction. According to the optical-transition selection rule,[10] although the spin polarization of the photogenerated conduction electrons is 0% for linearly polarized light, it is 50% for circularly polarized light. Therefore, defect electron spins are not polarized for linearly polarized light but are polarized for circularly polarized light. Consequently, the conduction electron population depends on the excitation light polarization, which generates a photoconductivity difference. The relationship between the conduction electron population and the excitation light polarization is presented in the supplementary material. Previous work developed a polarization-sensitive photoconductor;[6] however, photodiodes are preferable in terms of dark current, noise, and response time. In photodiodes, the capture efficiency of conduction electrons by defect states can vary with the bias voltage-dependent band potential. The spin polarization of defect electrons is dependent on the light intensity. In this study, we developed a near-infrared photodiode based on GaNAs and studied the influence of the light power and bias voltage on the polarization-dependent photocurrent characteristics.

The sample structure of the GaNAs-based photodiode and the measurement setup are shown in Fig. 1(a). The semiconductor layers were grown on a *p*-GaAs (100) substrate using radio frequency plasma-assisted molecular beam epitaxy (MBE). The semiconductor structure comprises of *p*-GaAs:Zn (100) substrate ($p = 1 \times 10^{19}\,\mathrm{cm}^{-3}$)/200-nm *p*-GaAs:Be ($p = 1 \times 10^{18}\,\mathrm{cm}^{-3}$)/100-nm *p*-$Al_{0.3}Ga_{0.7}As$:Be ($p = 1 \times 10^{18}\,\mathrm{cm}^{-3}$)/20-nm *p*-GaAs:Be ($p = 1 \times 10^{18}\,\mathrm{cm}^{-3}$)/200-nm *i*-GaNAs/20-nm *n*-GaNAs:Si ($n = 2 \times 10^{17}\,\mathrm{cm}^{-3}$). The nitrogen content of the GaNAs layers was set to approximately 2% by adjusting the radio frequency power and N_2 flow rate. The *n*-GaNAs layer was grown at 400 °C because the low-temperature growth tends to introduce Ga^{2+} interstitials that behave as spin-filtering defects.[9] The *i*-GaNAs layer, which behaves as the main light-absorbing layer, was grown at 450 °C to obtain sufficient photocurrent via reducing the defect density. To prevent non-uniform nitrogen distribution due to growth interruption and degradation of crystal quality due to ion-induced damage during growth interruption,[11] the substrate temperature was reduced before the *i*-GaNAs layer growth was completed. This growth scheme allows the *i*-GaNAs and *n*-GaNAs layers to grow without interruption. The other semiconductor layers were grown at 560 °C. After the semiconductor layer growth, the surface was passivated with As and transferred by air to another growth system consisting of MBE and electron beam (EB) deposition. After thermal desorption of the As capping layer, the MgO layer was grown at 300 °C by EB deposition.[12,13] The sample was then transferred to another EB system by air to grow a Fe (10 nm)/Au (3 nm) electrode. Before the growth, the sample was annealed in an oxygen atmosphere.[12] Finally, the standard photolithography and etching techniques were used to fabricate conventional photodiodes. Since no magnetic field was applied in this study, the Fe layer was used as a normal metallic electrode rather than a spin detection electrode in a spin photodiode. Although the 10-nm-thick Fe film is expected to exhibit an in-plane magnetization, the influence of the magneto-optical effect on the polarization-dependent photocurrent characteristics is small in this study, as described in the supplementary material. The MgO tunneling layer

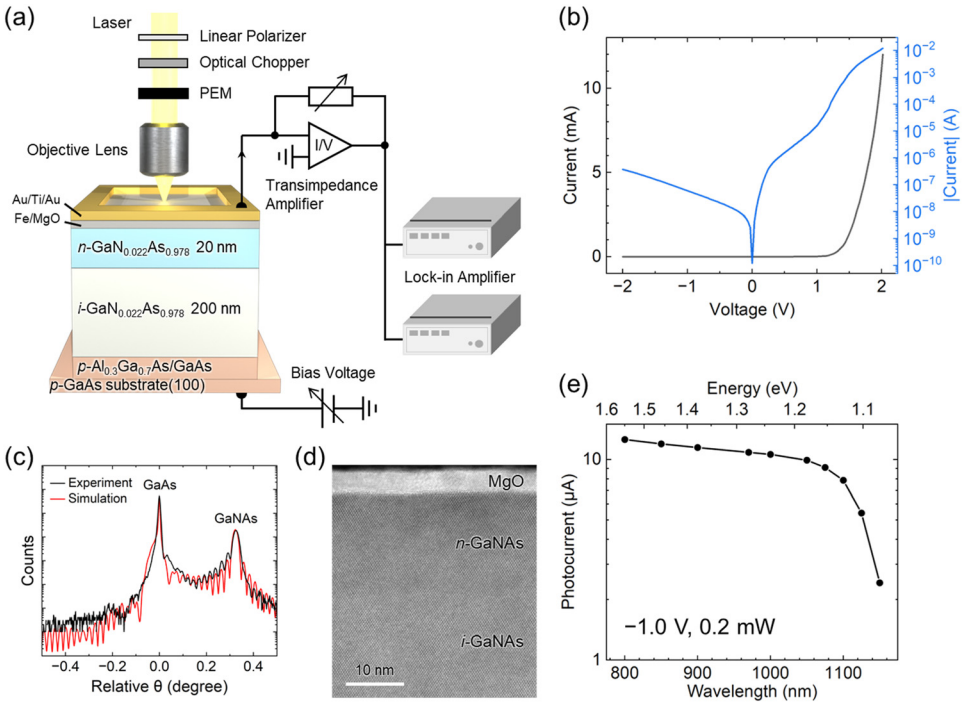


FIG. 1. (a) Schematic of GaNAs-based photodiode and measurement setup of polarization-dependent photocurrent. (b) *I*–*V* characteristics of the developed photodiode. (c) Experimental and simulated XRD θ–2θ scans of the sample across the GaAs(004) reflection. (d) High-resolution BF-STEM image of GaNAs layers. (e) Photocurrent as a function of laser wavelength at −1.0 V with a laser power of 0.2 mW.

09 July 2025 02:04:27

Published under an exclusive license by AIP Publishing

is expected to increase the capture efficiency of conduction electrons by defect states via the increase in the extraction time of the conduction electrons to the electrode.

All the photocurrent measurements were performed at room temperature without a magnetic field. The light intensity and polarization of the pulsed laser were modulated using an optical chopper (509 Hz) and a photoelastic modulator (PEM, 51 kHz), respectively. The incident light was periodically changed from linear to elliptical and to circular polarization. The laser was then focused using an objective lens and incident on the sample. The polarization-independent photocurrent (i_{photo}) and polarization-dependent photocurrent (Δi) were detected using lock-in amplifiers. To measure Δi, the 2f component (twice the modulation frequency of the PEM) was detected. The I–V characteristics of the photodiode are shown in Fig. 1(b). This exhibits the typical diode characteristics of a p-i-n junction.[14] The generation-recombination current is the main transport process from 0.3 to 0.8 V, whereas the electron-diffusion current is dominant from 1.0 to 1.4 V. The current at low bias voltages originates from the recombination and generation of carriers through the intermediate states formed by impurities in the depletion layer. No noticeable leakage currents are observed.

Figure 1(c) presents experimental and simulated θ-2θ x-ray diffraction (XRD) scans across the GaAs(004) reflection. The GaNAs peak exhibited well-defined interference fringes, indicating abrupt epitaxial interfaces. Fitting analysis determined the nitrogen content in the GaNAs layer to be 2.2%, suggesting a coherently strained layer with a homogeneous nitrogen distribution. These results confirmed the high epitaxial quality of the samples with sharp interfaces. A high-resolution bright-field scanning transmission electron microscopy (BF-STEM) image of the GaNAs layers is shown in Fig. 1(d). Since no growth interruption was employed for the two GaNAs layers, no interface damage was observed, indicating the formation of a high epitaxial quality and sharp interface. These XRD and BF-STEM results suggest that potential fluctuations caused by inhomogeneous nitrogen distribution and the formation of unintentional defects, which can affect the photocurrent characteristics, are suppressed. The i_{photo} as a function of laser wavelength at −1.0 V with a laser power of 0.2 mW is shown in Fig. 1(e). i_{photo} decreased sharply above 1100 nm. This is due to a significant decrease in the bandgap with increasing nitrogen content.[15] The photosensitive wavelength could be tuned by varying the nitrogen content of GaNAs. According to a previous study,[16] the bandgap of $GaN_{0.022}As_{0.978}$ is estimated to be 1.12 eV (1107 nm). This result indicated that an energy gap was achieved in the GaNAs layers, as expected. In the experiments described below, the laser wavelength was set to 1075 nm, at which sufficient photocurrent could be obtained. Here, no photocurrent peak corresponding to the bandgap of GaNAs was observed. This can be due to the used pulsed laser with a full width at half maximum of ∼10 nm. i_{photo} increased slightly at shorter wavelengths. This tendency may be related to the absorption coefficient depending on the wavelength. The absorption coefficient of GaNAs increases with the decrease in the wavelength.[17] In general, as the absorption coefficient increases, the photocurrent tends to increase.

The temporal variations of the photocurrent at −0.5 V with a laser power of 3.0 mW and of normalized PEM reference signal are presented in Figs. 2(a) and 2(b), respectively. A distinct photocurrent difference was observed between circularly and linearly polarized light. The intermediate photocurrent values appear for elliptically polarized light. This result demonstrates that the discrimination between circularly and linearly polarized light can be achieved at room temperature without a magnetic field in a GaNAs-based photodiode. Here, the figure of merit of the light polarization discrimination is defined as

$$F = (i^{\sigma_{cir}} - i^{\sigma_{lin}})/(i^{\sigma_{cir}} + i^{\sigma_{lin}}) = \Delta i/2i_{photo}, \quad (1)$$

where $i^{\sigma_{cir}}$ and $i^{\sigma_{lin}}$ are the photocurrents for circularly and linearly polarized light, respectively. The bias voltage dependences of i_{photo}, Δi, and F measured with laser powers of 0.2 and 2.0 mW are shown in Figs. 2(c) and 2(d), respectively. The trends in i_{photo} and F were similar at both powers. As the reverse bias voltage increases, i_{photo} increases,

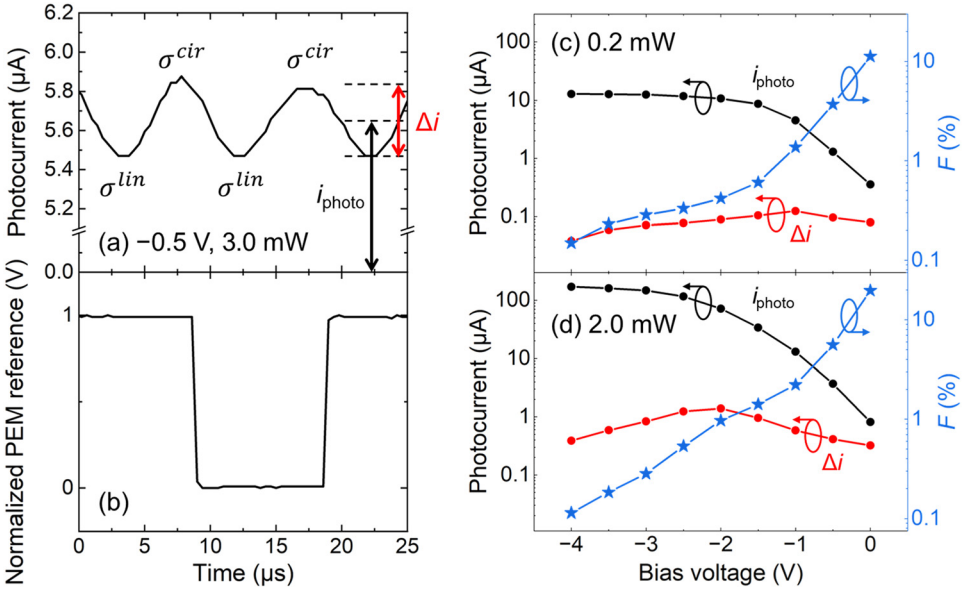


FIG. 2. Temporal variations of (a) photocurrent for different light polarization at −0.5 V with a laser power of 3.0 mW and of (b) normalized PEM reference signal. The definitions of i_{photo} and Δi are also indicated in (a). Bias voltage dependences of i_{photo}, Δi, and F with laser powers of (c) 0.2 mW and (d) 2.0 mW.

09 July 2025 02:04:27

Published under an exclusive license by AIP Publishing

whereas F decreases. The increase in i_{photo} is due to the efficient extraction of carriers to the electrode as the band potential tilt increases. In contrast, Δi exhibited a maximum at -1.0 V for 0.2 mW and at -2.0 V for 2.0 mW, decreasing as the reverse bias voltage further increased. Increasing the reverse bias voltage is expected to increase both i_{photo} and Δi; however, spin relaxation of conduction electrons can be accelerated under a strong electric field. Spin depolarization in GaAs can be enhanced due to D'yakonov–Perel' spin relaxation as a result of the electric-field-induced increase in the electron temperature.[18] The spin depolarization enhanced by electric field is also expected to occur in GaNAs. In this case, the capture of conduction electron spins by the defect states tends to weaken, as discussed below. The spin-selective capture of conduction electrons is suppressed, resulting in the decreased Δi. By increasing the laser power, a sufficient number of conduction electrons can be captured by the defect states to polarize the defect electron spins even at large reverse bias voltages. Therefore, the maximum of Δi would appear at the larger reverse bias voltage.

The dependence of F on the laser power at different bias voltages was measured, as shown in Fig. 3(a). F increased with the laser power at all bias voltages. This result agrees with the excitation-power dependence of the photoluminescence polarization of GaNAs.[9,19] This is due to the promoted cycle of electron spin capture by the defect states and the recombination of defect electron spins with holes. The slope of the increase in F and maximum of F depended on the bias voltage. To reveal the influence of the reverse bias voltage on F, based on previous studies,[5,19,20] we performed a coupled rate equation analysis of the power-dependent F using Eqs. (2)–(4). The rate equation model is schematically illustrated in Fig. 3(b),

$$\frac{dn_{\uparrow/\downarrow}}{dt} = G_{\uparrow/\downarrow} + \frac{n_{\downarrow/\uparrow} - n_{\uparrow/\downarrow}}{2\tau_s} - \gamma_e n_{\uparrow/\downarrow} N_{\downarrow/\uparrow} - \frac{n_{\uparrow/\downarrow}}{\tau_e}, \tag{2}$$

$$\frac{dN_{\uparrow/\downarrow}}{dt} = \frac{N_{\downarrow/\uparrow} - N_{\uparrow/\downarrow}}{2\tau_{sc}} - \gamma_e n_{\downarrow/\uparrow} N_{\uparrow/\downarrow} + \frac{1}{2}\gamma_h p N_{\uparrow\downarrow}, \tag{3}$$

$$\frac{dp}{dt} = G_{\uparrow} + G_{\downarrow} - \gamma_h p N_{\uparrow\downarrow}. \tag{4}$$

Here, $n_{\uparrow/\downarrow}$ represents the density of conduction electrons with up-spin/down-spin and $N_{\uparrow/\downarrow}$ represents the density of Ga^{2+} defects occupied by an unpaired electron with up-spin/down-spin. $N_{\uparrow\downarrow}$ is the density of Ga^{+} defects occupied by two spin-paired electrons and N_c is the total density of Ga interstitial defects ($N_c = N_{\uparrow} + N_{\downarrow} + N_{\uparrow\downarrow}$). p is the density of free holes, and $p = n_{\uparrow} + n_{\downarrow} + N_{\uparrow\downarrow}$ from the requirement of charge neutrality. γ_e (γ_h) denotes the capture coefficient of conduction electrons (free holes) by the Ga interstitial defects. τ_s and τ_{sc} denote the spin relaxation time of conduction electrons and Ga^{2+} defect electrons, respectively. τ_e is the extraction time of the conduction electrons to the electrode. Here, $G_{\uparrow/\downarrow} = G_{opt}(1 \pm P_0)/2$ implies the optical generation rate of conduction electrons for the corresponding spin states. G_{opt} is the optical generation rate of the total conduction electrons and P_0 is the initial spin polarization of the photogenerated electrons. Based on the optical-transition selection rule,[10] P_0 was set to 0.5 and 0 for circularly and linearly polarized light, respectively. τ_{sc} was set to 800 ps based on the previous studies.[19,21] Since hole mobility in GaNAs is much lower than electron mobility,[22–25] the effect of drift on γ_h can be negligible compared to γ_e. γ_h was assumed to be constant with respect to the bias voltage. Note that the hole current should be sufficiently small compared with the electron current because the $Al_{0.3}Ga_{0.7}As$ barrier exists only on the p-layer side. Therefore, the photogenerated electron current (photocurrent) for circularly and linearly polarized light can be defined as[5]

$$i^{\sigma_{cir(lin)}} = e\left(\frac{n_{\uparrow}^{\sigma_{cir(lin)}} + n_{\downarrow}^{\sigma_{cir(lin)}}}{\tau_e}\right). \tag{5}$$

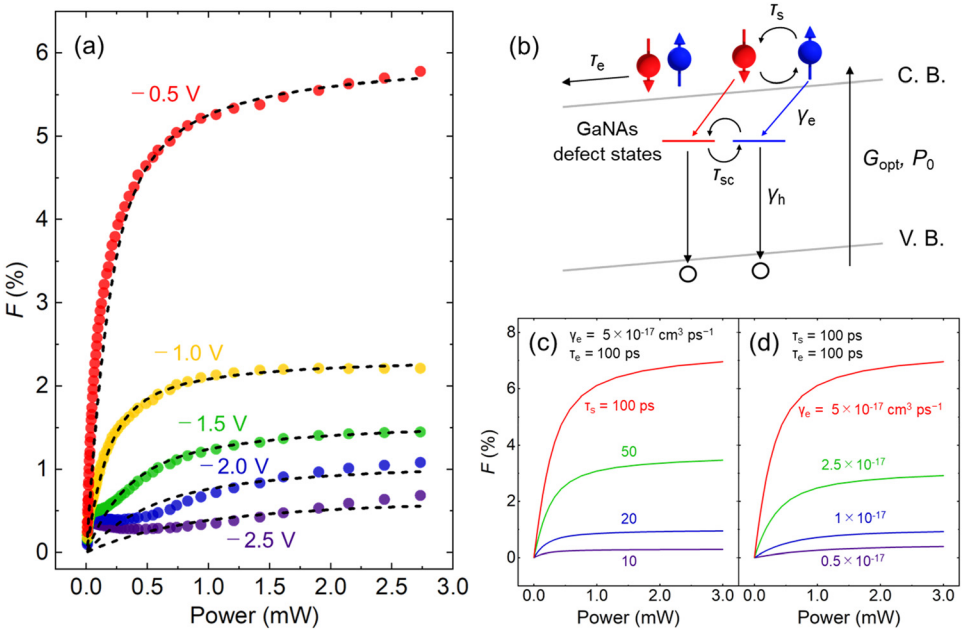


FIG. 3. (a) Power dependence of F at different bias voltages. The dashed lines indicate the best-fitted curves of rate equation. (b) Rate equation model considering optical generation of conduction electron spins, extraction of conduction electrons, and capture of conduction electrons by defect states. Simulations of rate equation with various (c) τ_s and (d) γ_e.

09 July 2025 02:04:27

Published under an exclusive license by AIP Publishing

Hence, F can be calculated as the ratio of the conduction electron densities for circularly and linearly polarized light.

Figure 3(c) presents the simulation results of the rate equation with various τ_s at fixed parameters of $\gamma_e = 5 \times 10^{-17}\,\mathrm{cm^3\ ps^{-1}}$ and $\tau_e = 100$ ps. The decrease in τ_s leads to a decreased spin polarization of conduction electrons captured by the defect states. In this case, the spin-selective capture of conduction electrons by the defect states was weakened, resulting in a decrease in F. The simulation results with various γ_e at $\tau_s = \tau_e = 100$ ps are presented in Fig. 3(d). The decrease in γ_e also causes a decrease in F. The effects of τ_s and γ_e on the power-dependent F appear to be the same, but γ_e tends to change the power required to increase F. The increase in F became slower as γ_e decreased. The decrease in γ_e reduces the cycle of spin capture and recombination, which causes a dynamic polarization of the defect electron spins. Hence, a higher power is required to promote the dynamic polarization process. The best-fit results of the rate equation for power-dependent F are shown in Fig. 3(a). The sharp and slow increases in F at low and high reverse bias voltages were well fitted by optimizing the parameters. The fitting results yielded $N_c = 5.3 \times 10^{14}\,\mathrm{cm^{-3}}$ and $\gamma_h = 4.0 \times 10^{-16}\,\mathrm{cm^3\ ps^{-1}}$. These values are relatively close to those reported for GaNAs.[19,21] This indicates the validity of the fitting. The deviations between the fitting results and the experimental values in the low-power region are discussed in the supplementary material.

The bias voltage dependences of τ_s, γ_e, and τ_e, as deduced from the rate equation fitting, are summarized in Figs. 4(a)–4(c). All of these values decreased with increasing reverse bias voltage. This result can be explained by the bias voltage-induced change in the conduction potential. The one-dimensional calculated conduction profiles of the GaNAs layers at −0.5 and −2.5 V are shown in Figs. 4(d) and 4(e), respectively. In this calculation, the MgO/Fe interface was set as the origin of the position. The calculations were performed using the nextnano software.[26] At a relatively low electric field of −0.5 V, not only are electron spins generated by circularly polarized excitation less subjected to the electric-field-induced spin relaxation, but also the spin polarization of conduction electrons captured by the defect states tends to be high, as depicted in Fig. 4(d). The resulting high-spin polarization of defect electrons activates the SDR effect. This explanation is reflected in the longer τ_s and larger γ_e at lower reverse bias voltages. The presence of MgO tunneling barrier may also increase γ_e via the increase in τ_e. In this case, the conduction electron density for circularly polarized light was larger than that for linearly polarized light, resulting in a higher F. In contrast, the spin polarization of the conduction electrons can be rapidly lost with an increase in the electric field,[27] as depicted in Fig. 4(e). Spin-polarized conduction electrons photogenerated far from the electrode are likely to lose spin polarization during transport to the n-GaNAs layer with high-density defect states. This phenomenon is reflected in the shortest τ_s at −2.5 V. In addition, the decrease in τ_e with increasing drift velocity can reduce γ_e because it enhances the extraction of conduction electrons to the electrode. These factors reduce the spin polarization of defect electrons for circularly polarized light by deactivating the SDR effect. As a result, the spin polarization of the conduction electrons and defect electrons approaches 0%, as in the case of linearly polarized light, and thus, F decreases at higher reverse bias voltages. These results suggest a trade-off between the discrimination efficiency of light polarization and the response time of the polarization-sensitive photodiode based on the SDR effect.

Finally, we compare the performance between this work and existing polarization-sensitive photodetectors. Some kinds of materials, including organic semiconductor,[28–30] perovskite,[31,32] and dilute nitride semiconductor,[6] have been applied in polarization-sensitive photodetectors (supplementary Table S1). The photodetectors based on the chiral materials exhibit high photoresponsivity and low dark current. However, most of the chiral materials exhibit a low carrier mobility on the magnitude of 10^{-5}–$10^{-3}\,\mathrm{cm^2/V\,s}$,[29] making them unsuitable for high-speed operation. GaNAs-based photodiode in this study exhibits a low photoresponsivity due to the presence of the MgO tunneling barrier but exhibits a low dark current comparable to the existing polarization-sensitive photodetectors. A remarkable performance parameter is the response time expected from the rate equation analysis. In the case of a photodiode, the response time corresponds roughly to the extraction time of the conduction electrons

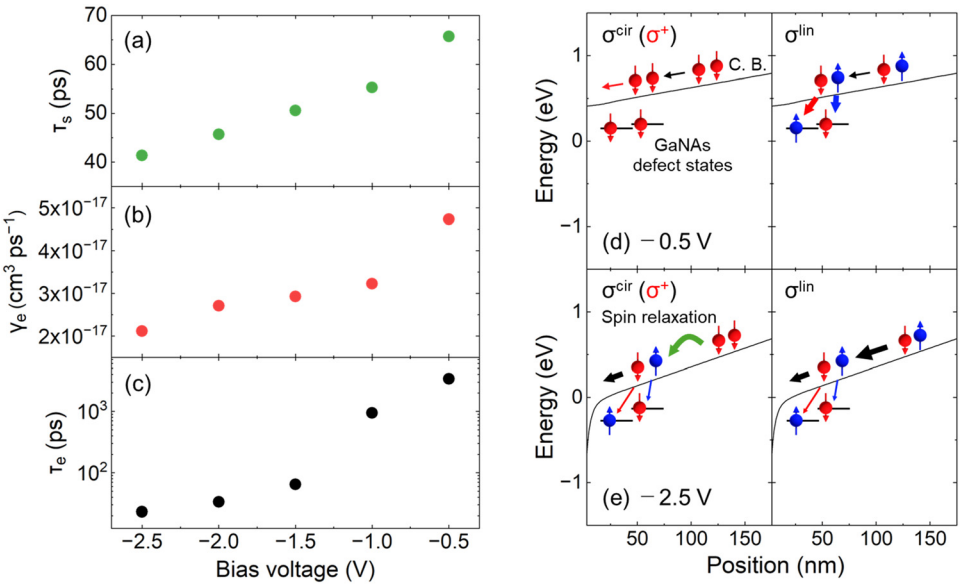


FIG. 4. Bias voltage dependences of (a) τ_s, (b) γ_e, and (c) τ_e, deduced from rate equation analysis. Schematic of electron spin dynamics for circularly polarized (σ^+) and linearly polarized light with one-dimensional calculated conduction band profiles of GaNAs layers at (d) −0.5 V and (e) −2.5 V. The energy positions of GaNAs defect states are hypothetical.

09 July 2025 02:04:27

Published under an exclusive license by AIP Publishing

to the electrode, τ_e, obtained by rate equation analysis. τ_e was estimated to be 3.4 ns and 34 ps at −0.5 and −2.0 V, respectively. Therefore, the developed photodiode based on GaNAs has a significant advantage in terms of high-speed operation over the existing polarization-sensitive photodetectors. Furthermore, considering that F reached 1% even at −2.0 V, these findings suggest that the developed polarization-sensitive photodiode can operate at 10 GHz.

In summary, the polarization-dependent photocurrent characteristics of a GaNAs-based near-infrared photodiode were investigated at room temperature without a magnetic field. The discrimination efficiency between the circularly and linearly polarized light depends on the laser power and bias voltage. At −2.0 V, where the discrimination efficiency reached 1%, the extraction time of the conduction electrons to the electrode was estimated to be 34 ps. This result suggests that the developed polarization-sensitive photodiode can operate at ten GHz. The higher discrimination efficiency at higher power was attributed to the activated spin-selective capture of conduction electrons by the defect states in the case of circularly polarized light. The lower discrimination efficiency at higher reverse bias voltages was due to an increase in the electric field. The high electric field not only accelerates the spin relaxation of conduction electrons but also promotes the extraction of conduction electrons to the electrode, leading to a decrease in the spin polarization of the captured electrons and the capture efficiency of the conduction electrons. These factors suppress the dynamic polarization of the defect electron spins; thus, the spin-selective capture of conduction electrons by the defect states is weakened. This study provides a comprehensive understanding of polarization-sensitive photodiodes based on the spin-dependent recombination effect of GaNAs.

See the supplementary material for details on the relationship between the conduction electron population and excitation light polarization, the influence of the magneto-optical effect on the polarization-dependent photocurrent characteristics, the deviations between the fitting results and the experimental values of power-dependent F in the low-power region, and the performance comparison between this work and existing polarization-sensitive photodetectors.

This work was financially supported by JSPS KAKENHI (Nos. JP20K20433, JP21H01356, JP21KK0068, JP23K26153, and JP24K00913), JST FOREST (Grant No. JPMJFR202E), JST ALCA-Next (Grant No. JPMJAN23E5), and NEDO (Grant No. P14004). A part of this work was conducted at Joint-Use Facilities: Laboratory of Nano-Micro Material Analysis and High-Voltage Electron Microscope Laboratory, supported by "Nanotechnology Platform Program" and "Advanced Research Infrastructure for Materials and Nanotechnology in Japan (ARIM)" of the Ministry of Education, Culture, Sports, Science and Technology (MEXT), Grant No. JPMXP1222HK0049 (Hokkaido University).

AUTHOR DECLARATIONS

Conflict of Interest

The authors have no conflicts to disclose.

Author Contributions

Daiki Mineyama: Conceptualization (equal); Data curation (equal); Formal analysis (lead); Investigation (lead); Methodology (equal); Writing – original draft (lead). **Tatsuya Yano:** Formal analysis (supporting); Investigation (equal); Methodology (supporting); Writing – review & editing (supporting). **Kohei Etou:** Data curation (supporting); Investigation (supporting); Methodology (supporting); Resources (supporting); Writing – review & editing (supporting). **Kaito Nakama:** Investigation (supporting); Resources (equal); Writing – review & editing (supporting). **Hidetoshi Hashimoto:** Investigation (supporting); Resources (equal); Writing – review & editing (supporting). **Keisuke Minehisa:** Investigation (supporting); Resources (equal); Writing – review & editing (supporting). **Junichi Takayama:** Data curation (supporting); Methodology (supporting); Software (equal); Writing – review & editing (supporting). **Agus Subagyo:** Resources (equal); Writing – review & editing (supporting). **Kazuhisa Sueoka:** Resources (supporting); Writing – review & editing (supporting). **Fumitaro Ishikawa:** Investigation (supporting); Resources (equal); Writing – review & editing (equal). **Akihiro Murayama:** Conceptualization (supporting); Funding acquisition (equal); Methodology (supporting); Project administration (supporting); Supervision (supporting); Writing – review & editing (supporting). **Satoshi Hiura:** Conceptualization (lead); Data curation (equal); Funding acquisition (equal); Methodology (equal); Project administration (lead); Supervision (lead); Writing – review & editing (lead).

DATA AVAILABILITY

The data that support the findings of this study are available from the corresponding author upon reasonable request.

REFERENCES

[1]P. A. Dainone, N. F. Prestes, P. Renucci, A. Bouché, M. Morassi, X. Devaux, M. Lindemann, J.-M. George, H. Jaffrès, A. Lemaitre, B. Xu, M. Stoffel, T. Chen, L. Lombez, D. Lagarde, G. Cong, T. Ma, P. Pigeat, M. Vergnat, H. Rinnert, X. Marie, X. Han, S. Mangin, J.-C. Rojas-Sánchez, J.-P. Wang, M. C. Beard, N. C. Gerhardt, I. Žutić, and Y. Lu, Nature **627**, 783 (2024).
[2]M. Lindemann, G. Xu, T. Pusch, R. Michalzik, M. R. Hofmann, I. Žutić, and N. C. Gerhardt, Nature **568**, 212 (2019).
[3]P. E. Faria Junior, G. Xu, J. Lee, N. C. Gerhardt, G. M. Sipahi, and I. Žutić, Phys. Rev. B **92**, 075311 (2015).
[4]R. Farshchi, M. Ramsteiner, J. Herfort, A. Tahraoui, and H. T. Grahn, Appl. Phys. Lett. **98**, 162508 (2011).
[5]V. I. Safarov, I. V. Rozhansky, Z. Zhou, B. Xu, Z. Wei, Z.-G. Wang, Y. Lu, H. Jaffrès, and H.-J. Drouhin, Phys. Rev. Lett. **128**, 057701 (2022).
[6]R. S. Joshya, H. Carrère, V. G. Ibarra-Sierra, J. C. Sandoval-Santana, V. K. Kalevich, E. L. Ivchenko, X. Marie, T. Amand, A. Kunold, and A. Balocchi, Adv. Funct. Mater. **31**, 2102003 (2021).
[7]V. K. Kalevich, E. L. Ivchenko, M. M. Afanasiev, A. Y. Shiryaev, A. Y. Egorov, V. M. Ustinov, B. Pal, and Y. Masumoto, J. Exp. Theor. Phys. Lett. **82**, 455 (2005).
[8]Y. Puttisong, X. J. Wang, I. A. Buyanova, H. Carrére, F. Zhao, A. Balocchi, X. Marie, C. W. Tu, and W. M. Chen, Appl. Phys. Lett. **96**, 2010 (2010).
[9]X. J. Wang, I. A. Buyanova, F. Zhao, D. Lagarde, A. Balocchi, X. Marie, C. W. Tu, J. C. Harmand, and W. M. Chen, Nat. Mater. **8**, 198 (2009).
[10]F. Meier and B. Zakharchenya, *Optical Orientation* (Elsevier, North Holland, Amsterdam, 1984).
[11]L. H. Li, Z. Pan, W. Zhang, Y. W. Lin, X. Y. Wang, R. H. Wu, and W. K. Ge, J. Cryst. Growth **223**, 140 (2001).
[12]K. Etou, S. Hiura, S. Park, K. Sakamoto, J. Takayama, A. Subagyo, K. Sueoka, and A. Murayama, Phys. Rev. Appl. **16**, 014034 (2021).
[13]K. Etou, S. Hiura, S. Park, J. Takayama, A. Subagyo, K. Sueoka, and A. Murayama, Phys. Rev. Appl. **19**, 024055 (2023).
[14]E. Fred Schubert, *Light-Emitting Diodes*, 4th ed. (E. Fred Schubert, 2023).

09 July 2025 02:04:27

Published under an exclusive license by AIP Publishing

[15]M. Weyers, M. S. Michio Sato, and H. A. Hiroaki Ando, Jpn. J. Appl. Phys., Part 2 **31**, L853 (1992).
[16]I. Vurgaftman and J. R. Meyer, J. Appl. Phys. **94**, 3675 (2003).
[17]S. Turcotte, J. N. Beaudry, R. A. Masut, P. Desjardins, G. Bentoumi, and R. Leonelli, J. Appl. Phys. **104**, 083511 (2008).
[18]M. I. Miah, J. Phys. D. Appl. Phys. **41**, 159801 (2008).
[19]Y. Huang, V. Polojärvi, S. Hiura, P. Höjer, A. Aho, R. Isoaho, T. Hakkarainen, M. Guina, S. Sato, J. Takayama, A. Murayama, I. A. Buyanova, and W. M. Chen, Nat. Photonics **15**, 475 (2021).
[20]D. Lagarde, L. Lombez, X. Marie, A. Balocchi, T. Amand, V. K. Kalevich, A. Shiryaev, E. Ivchenko, and A. Egorov, Phys. Status Solidi **204**, 208 (2007).
[21]S. Hiura, S. Sato, S. Sakano, J. Takayama, and A. Murayama, Appl. Phys. Lett. **126**, 052403 (2025).
[22]A. Patanè, G. Allison, L. Eaves, M. Hopkinson, G. Hill, and A. Ignatov, J. Phys.: Condens. Matter **21**, 174209 (2009).
[23]M. Inagaki, K. Ikeda, H. Kowaki, Y. Ohshita, N. Kojima, and M. Yamagichi, Phys. Status Solidi C **10**, 589 (2013).
[24]J. Ibáñez, R. Cuscó, E. Alarcón-Lladó, L. Artús, A. Patanè, D. Fowler, L. Eaves, K. Uesugi, and I. Suemune, J. Appl. Phys. **103**, 103528 (2008).
[25]M. Reason, Y. Jin, H. A. McKay, N. Mangan, D. Mao, R. S. Goldman, X. Bai, and C. Kurdak, J. Appl. Phys. **102**, 103710 (2007).
[26]S. Birner, T. Zibold, T. Andlauer, T. Kubis, M. Sabathil, A. Trellakis, and P. Vogl, IEEE Trans. Electron Devices **54**, 2137 (2007).
[27]H. Sanada, I. Arata, Y. Ohno, Z. Chen, K. Kayanuma, Y. Oka, F. Matsukura, and H. Ohno, Appl. Phys. Lett. **81**, 2788 (2002).
[28]Y. Yang, R. C. da Costa, M. J. Fuchter, and A. J. Campbell, Nat. Photonics **7**, 634 (2013).
[29]D. Zhu, W. Jiang, Z. Ma, J. Feng, X. Zhan, C. Lu, J. Liu, J. Liu, Y. Hu, D. Wang, Y. S. Zhao, J. Wang, Z. Wang, and L. Jiang, Nat. Commun. **13**, 3454 (2022).
[30]H. Han, J. H. Choi, J. Ahn, H. Lee, C. Choi, W. Jung, J. Yeom, D. K. Hwang, B. J. Sung, and J. A. Lim, ACS Appl. Mater. Interfaces **15**, 57447 (2023).
[31]C. Chen, L. Gao, W. Gao, C. Ge, X. Du, Z. Li, Y. Yang, G. Niu, and J. Tang, Nat. Commun. **10**, 1927 (2019).
[32]X. Zhang, Y. Xu, A. N. Alphenaar, S. Ramakrishnan, Y. Zhang, A. J. Babatunde, and Q. Yu, ACS Nano **18**, 14605 (2024).

09 July 2025 02:04:27

Published under an exclusive license by AIP Publishing